Morell, Mariana; Vionnet, Carlos; Tassi, Pablo

Three-dimensional flow patterns at a river difluence on the alluvial system of the Paraná River, Argentina

Three-dimensional flow patterns at a river difluence on the alluvial system of the Paraná River, Argentina

Mariana I. MORELL, Carlos A. VIONNET
Centre for Water & Environmental Studies at FICH
UNL & CONICET
Santa Fe, Argentina
cvionnet@fich1.unl.edu.ar

Pablo A. TASSI
Laboratoire National d'Hydraulique et Environnement
EDF R&D
Chatou, France
pablo.tassi@edf.fr

***Abstract*— Whilst identification of secondary flows may be straightforward in open-channels with regular geometry and slowly varying plane curvature, it is not so in the case of natural meandering streams, whose boundaries are loose and irregular. Indeed, due to the continuously changing plan form and variable bed topography, the hydrodynamics of a natural meandering stream is rather complex. The flow field is strongly three-dimensional (3D), and in each cross-section of the meandering stream a cross-flow develops. Thus, on the basic flow there is superimposed a flow in the transverse direction which occupies the large part of the cross section, whose formation is understood in terms of the mechanical imbalance between the local elevation of the free surface and the centrifugal force induced by channel curvature. The behavior of the crosswise flow measured at the outlet of the Colastiné River, Argentina, where the flow diverts in two branches forming an almost T-shaped difluence, is briefly analyzed here with the open source code Telemac-3d. This communication reports the comparison of cross-flows captured with two acoustic Doppler current profiler (aDcp) in the study site against numerical solutions obtained with models of increasing complexity: i) hydrostatic 3D model, ii) full non-hydrostatic 3D model, in conjunction with the zero-equation and two-equations turbulence models.**

I. INTRODUCTION

In the last decades, theoretical [12,1] as well as experimental research [2,3] on circular open-channel flows have emerged with the hope of uncovering part of the mechanisms responsible for river meandering. Despite the abundant research available on the subject, insight into the relevant meander processes is still incomplete [6,3]. Just to describe various stages of channel development, numerical models require the ability to compute the interaction among bend flow, transport of bed sediments, and failure of erodible banks over a wide range of time-space scales [8,3].

It has long been known that in meandering open-channels, the flow curvature gives rise to secondary circulation resulting in the classical 3D helical motion, partially responsible for the bank erosion processes observed in natural channels [1,2,3,13]. Whilst identification of secondary flows may be straightforward in open-channels with regular geometry and slowly varying plane curvature, it is not so in case of natural streams, whose boundaries are loose and irregular. Due to the changing planform and bed topography, the hydrodynamics of a natural meandering stream is rather complex. A cross-flow is superimposed to the basic flow, whose formation is understood in terms of the mechanical imbalance between the local elevation of the free surface and the centrifugal force induced by channel curvature. Secondary currents indeed represents a local process that scales with channel width b and water depth h, and behaves different depending on the aspect ratio $\beta = b/h$ [9]. Most known field data related to cross-flow formation lies within $10 \leq \beta \leq 15$ [10].

The present paper focuses on the hydrodynamics of curved open-channel flows, whose accurate description is required for further understanding of river meandering. To that aim, the behaviour of the cross-flow measured at the outlet of the Colastiné River, where the flow diverts in two branches forming an almost T-shaped difluence (Fig. 1), is analyzed by comparing detailed field data with numerical results obtained from mathematical models of increasing complexity, as more mechanisms are brought into play.

Therefore, the present paper's objective is to report some preliminary comparison of cross-flows captured with two acoustic Doppler current profiler (aDcp) in the study site, where the incoming flow experiences an acute turn

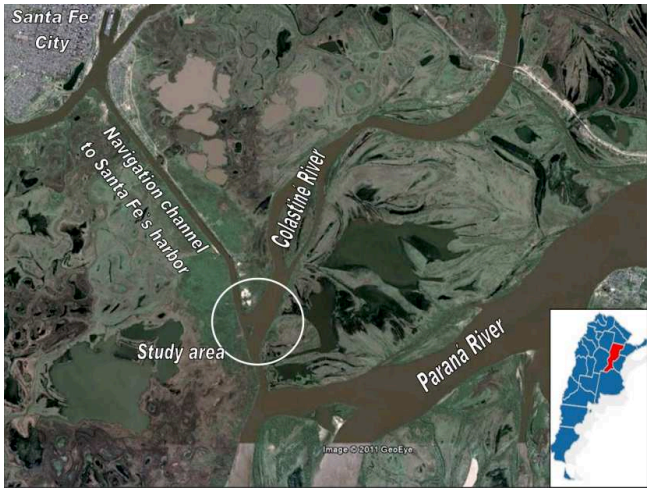

Figure 1. Study site on the alluvial system of the Paraná river, nearby Santa Fe city, Argentina.

which makes it prone to centrifugal effects, against numerical solutions obtained with 3D formulations tied to the zero-equation turbulence model (constant eddy viscosity value) and the two-equations standard k–ε model [5, 18, 22].

Next, a description of the mathematical models used are given first, starting with the classical explanation of the formation of a single cell of cross-stream circulation as reviewed by Engelund [1]. Then, few details of the 3D models are given since they are fully described elsewhere (see e.g. [18]), followed by the method used to capture field data. Preliminary results show that all models yield sounded solutions. Nevertheless, it is shown that in order to compute the figure of merit to characterize their performance, an unbiased treatment of the field data should be obtained first.

II. Materials & Methods

A. Mathematical Models

Many engineering problems involving water motion can be treated as shallow turbulent flows, where the shallowness condition $h/l << 1$, valid whenever the depth h of the water layer is small compared to the wavelike extent l of the fluid motion, is achieved. Flow in compound channels and coastal waters are just few examples of turbulent flows that can be analyzed with the shallow water assumption, also known as the long-wave approximation.

Two mathematical models describing the 3D velocity field (u,v,w) and the water depth h (bounded from below by a fixed bed and from above by a free surface), based upon the shallowness condition $h/l << 1$, are tested here numerically with two different formulations of Telemac-3d [18, 21]. The first one is a layered-average formulation obtained from the Navier-Stokes equations previously averaged in the sense of Reynolds (RANS), whereas the second refers to the full 3D RANS formulation [18]. Nevertheless, it is appropriated to highlight first the salient aspects of known analytical results on curved open-channel flows (see e.g. [1,7]).

1) Conceptual Model of Helical 3D Flow: The formation of a single cell of cross-stream circulation is well understood [12,1]. The long wave approximation reduces the fluid motion in vertical direction z to a mechanical balance between gravity and pressure, yielding the hydrostatic pressure distribution $g + \rho^{-1}\partial p/\partial z = 0$, where g is the acceleration of gravity, ρ the fluid density, and p the fluid pressure. Now, and with reference to Fig. 2, if (r, θ, z) are the cylindrical co-ordinates in radial, azimuthal, and upward directions, respectively, the radial velocity component, u_r, occurs in planes perpendicular to the primary-flow component u_θ, and is originated by the centrifugal acceleration u_θ^2/r due to channel curvature. Then, a simple order of magnitude analysis [12] reduces the set of equations governing the flow on curved open-channels to

$$\frac{\partial(ru_r)}{\partial r} + \frac{\partial u_\theta}{\partial \theta} = 0 \qquad (1)$$

$$-g\frac{\partial z_w}{\partial r} + \frac{u_\theta^2}{r} + \varepsilon\frac{\partial^2 u_r}{\partial z^2} = 0 \qquad (2)$$

$$gS + \varepsilon\frac{\partial^2 u_\theta}{\partial z^2} = 0, \qquad (3)$$

where z_w is the free surface elevation above datum, ε is the eddy viscosity coefficient −assumed constant− and S is the longitudinal channel bed slope which satisfies $Sr = S_0 R$, where $S = -dz_b/rd\theta$ and S_0 is the slope along the channel centre at $r = R$. Here, z_b is the bed elevation above datum.

Direct integration of (3) yields a parabolic distribution for u_θ, resolved by Engelund [1] after assuming a free-slip velocity at the bed level. Then, since the stream-wise velocity component, u_θ, varies from nearly zero at the bed to a maximum value at or near the surface, centrifugal effects are greater near the surface and less intense toward the bed. The centrifugal force is mostly counterbalanced by the radial pressure gradient, which has been assumed to be dominated by a hydrostatic balance manifested as a local hydraulic gradient in radial direction, $\partial z_w/\partial r$ (known as the transverse elevation phenomenon of the free surface). The balance of both forces can hold only for a certain single element, situated somewhere close to the central portion of the water column and moving with a velocity equal to u_θ^P. For particles moving near the upper portion of the water column with velocity $u_\theta > u_\theta^P$, the centrifugal force will be greater than the hydrostatic pressure gradient. These particles will be conveyed away from the centre of curvature. On the contrary, particles situated in the lower portion of the water column, for which $u_\theta < u_\theta^P$, will be moving toward the centre of curvature (Fig. 2). Integration of (2) yields a polynomial of 6[th] degree that fits a distribution similar to the profile depicted in Fig. 2. From continuity considerations, a non trivial vertical velocity component u_z will develop near the lateral banks, and the velocity field will acquire a 3D helical flow pattern round the river bend.

A difficulty arises whenever the cross-stream is to be captured in the field, where the turbulent flow is far from being uniform and the bed geometry is irregular.

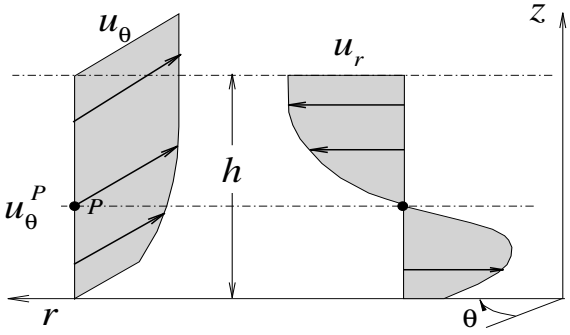

Figure 2. Single cell of cross-flow in curved open-channels.

2) Hydrostatic 3D Model: Giving the simple mechanical unbalance of forces that triggers the formation of a single cell of secondary circulation, it is natural to invoke the shallowness of the flowing water layer to approximate the vertical momentum equation with an hydrostatic balance of forces. Additional hypotheses support the use of constant eddy viscosity for the prediction of turbulence mixing, as

well as the so-called Boussinesq approximation where the variation of density is neglected everywhere except in the buoyancy term, if any, allowing thus for a linear change between temperature differences at bottom and top of each fluid layer. The remaining momentum conservation laws at each layer in the horizontal directions are to be solved in combination with the layer-averaged continuity equation

$$w_{upper} = -\frac{\partial u \Delta h}{\partial x} - \frac{\partial v \Delta h}{\partial y} + w_{lower} \quad (4)$$

where (x,y) represents the Cartesian coordinates in the horizontal plane, and w_{upper} and w_{lower} are the vertical component of velocity at the upper and lower limits of each layer of size Δh, respectively. Finally, the solution of the overall mass-conservation law yields the water depth, and with it, the position of the free surface. A detailed description of this type of model can be found in [4, 18].

3) Full 3D RANS Model: The governing equations can be found elsewhere [see e.g. 18, 21], which are essentially the full 3D Navier-Stokes equations previously averaged in the sense of Reynolds, albeit with the pressure force term split here into a hydrostatic component and a dynamic component, p_d:

$$p = p_{atm} + \rho_0 g \left[(z_w - z) + \int_z^{z_w} \frac{\Delta\rho}{\rho_0} dz \right] + p_d \quad (5)$$

This splitting is required not only to inherit part of the shallowness condition invoked before, but also for its intrinsic numerical stability advantages when there is a trade-off between the static pressure force component and the local gradient of the free surface [11]. Above, p_{atm} is the atmospheric pressure, and ρ_0 a fluid density reference value.

B. Field Data Adquisition

1) Study site: Field measurements at the study site along predetermined transects are being conducted periodically since 2004, where the Colastiné River diverts in two branches (Fig. 3). One of this branches leads to the Santa Fe's city harbour through a channel excavated artificially at the beginning of the XXth century. As a consequence of this "artificially" induced river curvature, the incoming flow from the Colastiné River experiences an acute turn at the channel inlet which makes it prone to inertial effects by centripetal forces. The field site is within the alluvial system of the Paraná River (Fig. 1), which is a large low gradient sandy river with a water surface elevation drop of the order of 3 to 5 cm per km, i.e., $(3-5)\times10^{-5}$. The river bed is characterized by fine and medium size sands, with banks composed of approximately 4-6 m layer of clay and silt overlying coarse sands.

2) Field Equipment: Two different aDcp have been used systematically mostly in low-medium flow conditions (Table 1), a SonTek RiverSurveyor and TRDI Rio Grande operating at 1000 kHz and 1200 kHz, respectively. Water velocity and bathymetry data were collected using one of the aDcp in tandem with a digital 210 Hz Raytheon single beam echo-sounder, in turn coupled to a differential Global Positioning System (dGPS) receiver Leika with Real-Time Kinematic (RTK) technology, which provided centimetre-level accuracies in (x,y) and in z (±0.02 m in planar and ±0.04 m in vertical dimensions, respectively). For sake of simplicity, description of adopted field procedures are mostly restricted here to the Sontek aDcp, whose proprietary software package *RiverSurveyor* was used for data acquisition and integration with position information from the dGPS. Similar procedures were later followed for the TRDI Rio Grande. The aDcp were mounted on the side of a fiberglass-hull vessel of 6.4 m in length, when a combined bathymetry and flow velocity field survey were carried out using the moving vessel methodology [16, 17]. A second serial port to collect dGPS input signals was attached to the on-board computer during the surveys, whose geographical data were later converted to TM (Transverse Mercator) coordinates, whereas the aDcp internal compass and tilt sensor (roll/pitch) referred water velocities components in terms of East-North-Up (ENU) coordinates.

3) Flow Measurements: Exploratory measurements were taken on November 4, 2004, when the vessel surveyed few transects roughly orientated perpendicular to the expected primary flow direction. Then, once secondary cells were detected with the first version of an in-house computational code devised to process the field data, more careful campaigns for data collection were organized. On April 27, 2006, each cross section to be measured was drawn in advance following rays that departed from a virtual centre of curvature, and orientated approximately perpendicular to the true channel inner bank (Fig. 3). The virtual centre of curvature was defined by fitting a circle to the plan-form of the inner bank [15]. Then, the helmsman followed the drawn cross-sections as closely as possible during the surveys by tracking the vessel position in real time with the dGPS, keeping its velocity approximately to 1 ms^{-1} (Table 1). From that day on, data were collected whenever possible in accordance with the United States Geological Survey (USGS) protocol for discharge measurements and velocity surveys (at least four transects for a discharge measurement or the recommended six transects for a velocity survey [14]).

TABLE I. FIELD DATA TRIPS, z_w: WATER STAGE MEASURED AT SFE'S HARBOUR, Q: MEAN DISCHARGE AT CHANNEL INLET, V: MEAN-VESSEL VELOCITY, Δz: CELL (BIN) SIZE, AND Δt: SAMPLING INTERVAL

Date	Flow variables and aDcp parameters				
	z_w [m]	Q [m^3s^{-1}]	V [ms^{-1}]	Δz [m]	Δt [s]
2004[a]	11.35	856 ± 98	0.7	0.90	10
2006[a]	11.56	917 ± 101	0.7	0.50	5, 10
2007[a]	12.33	663 ± 116	1.5	1.10	10
2008[a]	10.83	622 ± 119	1.2	0.75	10
2009[a]	13.32	1083 ± 126	0.6	0.90	10
2010[b]	12.83	1096 ± 73	1.4	0.25	0.59

a. Sontek, b. TRDI

Intrinsic operational limitations of aDcp architecture renders them unable to measure near all cross-section boundaries. The Sontek aDcp used has a profiling capability ranging from 1.2 m to 40.0 m, with cell-sizes going from 0.25 m to 5.00 m, and minimum blanking distance of 0.7 m. The equipment was set with a minimum blind distance from the water surface to the centre of the first bin of 1 m approximately [≈ 0.7 m (blanking distance) + 0.2 m (probe submergence) + $\Delta z/2$]. With this setting, the blind distance at the top layer (near the free surface) and the less resolved bottom layer (near the riverbed) rendered an unmeasured depth ranging from 55% to 15% for water columns located in shallow and deep zones, respectively.

Other issue was related to the lateral coarseness of the data given the narrow width of the channel inlet. On the time spanned by the sampling interval, the aDcp profiles the water column hundreds of times, whose backscatter data is then properly averaged and assigned to each bin centre in vertical direction, and to the midpoint of the travelled distance Δs covered between time t and $t+\Delta t$. The lateral vessel displacement Δs can be stimated with the expression $\Delta s \approx V\Delta t$, where V is vessel speed (Table 1). For a fixed Δt, the higher V the coarser the water column is. However, as it is shown later, the window of bulk moving water scanned was large enough to capture cells of cross-flow.

C. *Digital Terrain Model Generation*

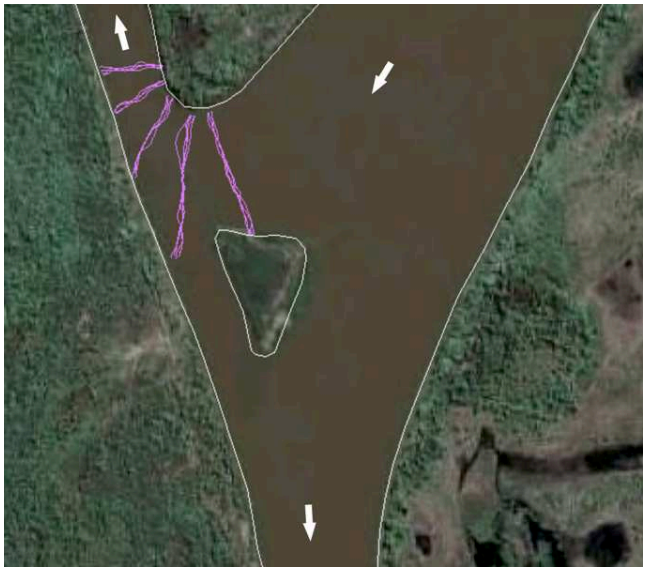

Figure 3. Cross-sections orientated perpendicular to inner bank.

The digital terrain model (DTM) of the computational domain represents the bare surface of the river bed, with a smooth transition between bed and riverbanks elevation data whenever possible. This is because the numerical modeling of open channel flows may encounter convergence difficulties nearby the physical boundaries of the computational domain due to contradictory data between river bottom elevation and local water depth. Therefore, an efficient data handling is an absolute requirement for the DTM generation process.

A semiautomatic approach to generate high quality DTM from scatter elevation points, surveyed from a moving boat with an echosounder and an aDcp both connected with a dGPS, and different procedures were bundle [27]. A data manager was developed based on separated steps to merge point data and line and polygon data from complementary sources and/or interfaces. This topographic data manager tool comprises the use of SMS (Surface Modelling System) developed by the EMRL at Brigham Young University [24], the visualization tool Tecplot [25] and a set of in-house routines written in Fortran 95 [27]. It allows the user to alter the outcome of the interpolation from the scatter data using different interaction tools and/or criteria, which may guide the user with the continuous assessment of the DTM generation process. The source data must be in plain ASCII format specifying (x,y,z), as defined above, with the inclusion of: i) the scatter set of bed elevation data, ii) the boundary data along riverbanks and limiting cross-sections in form of lines and polygons produced by the SMS, whose elevation is chosen by the user. Here, the scatter set of elevation data comprises isolate points collected along vessel paths with an echosounder, and depth data estimated through the four rays readings of the aDcp TRDI, corrected by roll and pictch with the aid of the VTM [26].

Then, an adaptive tessellation of the domain is constructed with a Delauney triangulation for the scatter point set. A Delaunay triangulation for a set P of points in the plane is a triangulation DT(P) such that no point in P is inside the circumcircle of any triangle in DT(P). Connecting the centers of the circumcircles produces the Voronoi diagram or Thiessen polygons of the surrounding scatter points, such that there is only one Thiessen polygon in the triangular irregular network (TIN) for each scatter point. The TIN so obtained, exported with Tecplot in ASCII format, enclosed a bounded domain that contains elements located outside some concave portion of the riverbanks. Those elements are then deleted by hand from the TIN data, and the scatter set of elevation data is interpolated using linear base functions onto a regular grid, whose size is defined by the user. The algorithm defines which node of the regular grid is wet (inside the domain) or dry (outside the domain), information that is later used to pass a 2D Laplacian kernel to smooth out the resulting interpolation. Then, a triangular finite element mesh (FEm) with the expected fine detail on critical areas, as well as fitted along internal boundaries where the flow has been measured in the field, is produced with SMS and later exported into Telemac format with an user specific interface [32]. The elevation data exported to Telemac is that of the regular grid containing both constant elevation points (outside the domain boundary), and highly accurate albeit properly smoothed bed data (inside the domain). The Fudaa interface of the open source Telemac System finally bounds the FEm with the exported bed bathymetry, mesh that is later used by Telemac-3d in the computations (Fig. 4).

D. *Finite Element Computations*

One of the reasons the Finite Element Method (FEM) is being increasingly used to study environmental problems

involving river and tidal flows is because its ability to ease the treatment of boundary conditions, bottom topographies and geometrically complex domains with high accuracy [23]. The 3D numerical codes used in this work belong to the open source Telemac System [18, 20], which solves the 3D Navier-Stokes equations with a FEM discretization under a hydrostatic and non-hydrostatic approximations [18, 21]. Telemac-3d is currently developed by the research and development department of Electricité de France (EDF) and the Telemac Consortium [20]. The Telemac-3d code has been fully parallelized using the Message Passing Interface paradigm (MPI).

The hydrostatic approximation consist on neglecting the vertical acceleration, diffusion and source term in the momentum equations. The non-hydrostatic approximation is based on the pressure decomposition into hydrostatic and hydrodynamic parts, allowing an accurate computation of the vertical velocity, which is now coupled with the whole system of equations. The overall algorithm for the solution of the hydrostatic 3D model is given hereafter: (i) computation of the advected velocity components by solving the advection terms in the momentum equations; (ii) determination of the new velocity components by taking into account the diffusion and source terms in the momentum equations (intermediate velocity field); (iii) computation of the water depth from vertical integration of the continuity equation and momentum equations by excluding the pressure terms; and (iv) determination of the vertical velocity w from the continuity equation and computation of the pressure step by the Chorin method [18]. The overall algorithm for the solution of the 3D non-hydrostatic model can be summarized as: (i) a hydrostatic part, which is almost exactly to the hydrostatic model described before, with the exception that the vertical velocity is also advected and diffused (in this step the free surface function is also determined); and (*ii*) a non-hydrostatic part, in which the velocity field is corrected by the dynamic pressure gradients in order to fulfil the divergence-free constraint [18, 21].

The 3D finite element mesh is obtained by first dividing the two-dimensional domain with non-overlapping linear triangles and then by extruding each triangle along the vertical direction into linear prismatic columns that exactly fit the bottom and the free-surface. In doing so, each column can be partitioned into non-overlapping layers, requiring that two adjacent layers comprise the same number of prisms. Turbulent stresses and turbulent fluxes are modelled using turbulent viscosity and turbulent gradient diffusion hypothesis, which introduce eddy viscosity and eddy diffusivity, respectively. Several turbulence-closure models are available in Telemac-3d [18]. Two turbulence closure models are used here: a constant eddy viscosity model and the standard k–ε turbulence model [5, 22].

In the present study, boundary conditions can be specified as follows: at the inflow boundary, all flow components are prescribed by imposing a velocity profile to provide a certain inflow discharge; at outlet boundaries, the normal gradients of all variables are set equal to zero. This homogeneous Neumann boundary condition implies that the surface integrals resulting from integration by parts in the variation formulation vanish. On the solid boundaries, the velocity tangential and normal to the boundary are set to zero. Finally, the position of the water surface is determined as described in [18, 21]. For the k–ε model, the boundary conditions are specified according to Burchard [22].

In all computations the domain is discretized with an unstructured triangular mesh consisting of 6623 triangular elements and 15 layers in the vertical direction, corresponding to 99,345 prisms. The time step is set equal to 0.1 s. For a given initial condition consisting on a water surface elevation of 13 m and velocity components equal to zero, the steady state is reached after about 100,000 time steps, corresponding to a physical time of about 2 hours 45'. For all simulations, the inflow discharge was 2416 m^3s^{-1} and a fixed surface elevation of 13 m was imposed at the outflow boundaries. When ran on eight processors of a Z600 HP workstation, the typical convergence time of the simulations presented in this paper was close to 35'.

E. Treatment of Field Data

Occasionally, reported results seem to be vague and open to different interpretations depending on the method

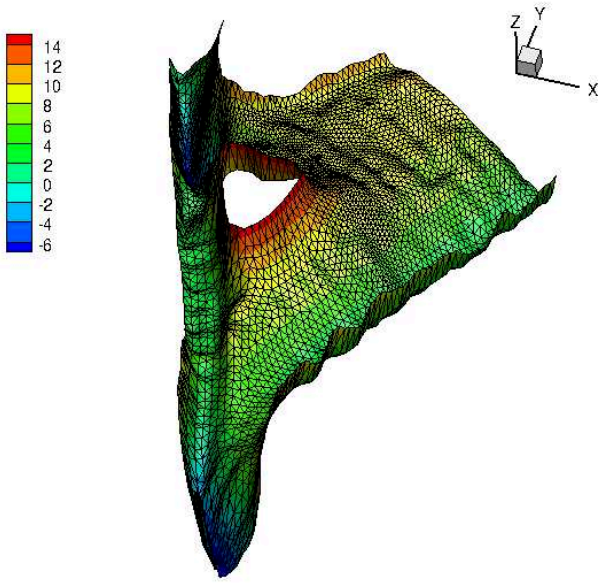

Figure 4. Finite element discretization of the computational domain.

used to extract secondary currents from the field data. The vast majority of researchers resort to the so-called Rozovskii method, which isolated the excess (or deficit) of the transverse velocity component relative to the respective depth-averaged value on any vertical profile. In brief, the method accounts for a rotation of the planar velocity vector with respect to the direction of the depth averaged velocity vector [12]. However, the procedure depends upon having zero net secondary discharge at the vertical, a condition normally used to close the mathematical problem posed by (1)–(3) albeit unrealistic in practical situations (where no fluid particle remains in the cross-wise plane as it is advected downstream by the primary flow).

Dinehart and Burau [14] proposed a method in two steps: firstly, a bend-crossing plane of velocity vectors from aDcp data is derived, secondly, elements of the backscatter intensity planes are used to guide an interactive alignment of the averaged velocity grids previously obtained. They found the bend-crossing plane through a section straightening procedure, where the velocity ensembles are spatially translated to a straight line defined by a mean crossing line fitted along multiple transects.

Two types of outputs are reported here, depending on the instrument used to capture the field data (Sontek or TRDI), and the algorithm used to extract the secondary currents from it. Usually, the procedure involves two steps, firstly using proprietary software, and then using some sort of an *ad hoc* software. For data captured with the TRDI aDcp, the 3D flow velocity data was first filtered and exported with the proprietary solftware *WinRiver II* [30], and later visualized with the VMT code [26]. In case the Sontek aDcp was used instead, the 3D flow velocity data was filtered and exported into spreadsheet files written in ASCII format with the aid of the proprietary *ViewADV* program [28]. These files were later processed with an in-house code written in Fortran 95 to get the transverse velocity field. The first version of the in-house code included: (1) conversion of coordinates from geographical to TM coordinates, (2) identification of data outliers, (3) generation of local coordinates along the cross-wise plane with reconstruction of the bed bathymetry.

The local ENU coordinates are formed from a plane tangent to the Earth's surface at the study site. Contrary to the usual convention of naming the east with *x*, and the north with *y*, the *RiverSurveyor* program measures water motion in 3D with *x/north*, *y/east*, and *z/up* [28]. Then, and as long as the collected data is corrected by the magnetic declination bias, both TM (Gauss-Krüger) and ENU coordinates are fully compatible, with the up component pointing out in the direction opposite to gravity.

The in-house coded developed for the Sontek aDcp data decomposes both the 2D planar (depth-averaged) and the full 3D vectors into tangential (along the cross-wise plane) and normal (along the stream-wise plane) components of the absolute velocity relative to ground, with the addition of the up component for the later case. Consequently, the field data collected along transects was always referred in geographical and ENU coordinates as well. The Gauss-Krüger coordinate system used by the Argentine Geographic Military Institute to make topographic maps of the national territory is based upon a TM projection, with origin of coordinates in the intersection of the South Pole with the central meridian of each band. Strict applications of the TM formulas, with south latitudes negative, results in the derivation of the correct easting and northing. Therefore, a module with the new World Geodetic System (WGS84) as the reference system was implemented, adopting the TM formulas given by Snyder [29] in combination with a procedure similar to that proposed by Dinehart and Burau [14] to project the 3D velocity field data. The location of the projection plane was dictated by the mean vessel trajectory during the surveys. The tangential and normal components were computed for each profile over the mean plane. Finally, both tangential and up components defined the projected cross-stream motion along the mean plane.

III. RESULTS

Curvilinear open-channel flows induce centrifugal forces which generate secondary currents and super-elevation of the water surface, which significantly may influence the 3D flow patterns since the cross-flow can be up to 40-50% of the bulk streamwise velocity. The selected surveyed cross-sections (XS) are showed in Fig. 5, numbering them from 0 (XS-0) at the upstream inlet boundary to 5 (XS-5) towards the downstream boundary in the navigation channel. It is seen in Fig. 6 that the secondary circulation is indeed strong, with transverse velocity on the order of 0.40 ms^{-1}, which is about 50% of the primary velocity component. The 2D velocity field depicted in Fig. 6 was captured during the 2009 campaign (Table 1) with the Sontek aDcp, and isolated according to the procedure aforementioned. The cross-stream flow pattern shown in Fig. 6 corresponds to cross-section 3 (XS-3), whose relative location within the computational domain is indicated in Fig. 5.

Fig. 7 shows cells of secondary motion captured with the

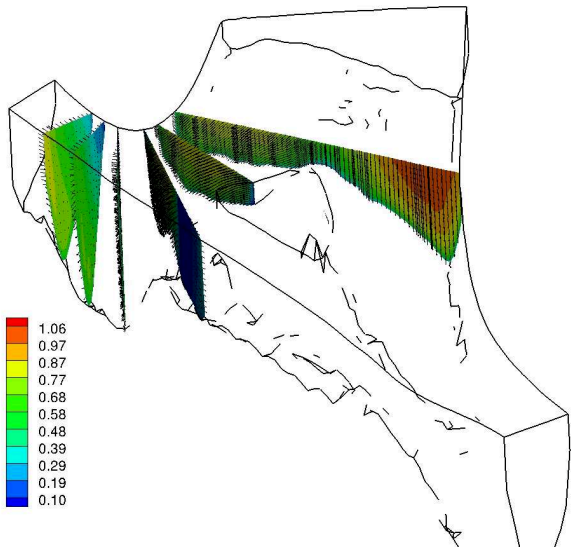

Figure 5. Computed secondary flow patterns at surveyed cross-sections

TRDI aDcp, plot produced with the VMT [26] toolbox. Here, it is worth to mention that VMT computes secondary currents according to the Rozovskii procedure, whose suitability to isolate cells of cross-flow from a skewed primary flow is now under close scrutiny among different authors [26, 31].

This reach of the river difluence, characterized by the strong asymmetry of the bed topography, and consequently, of the flow dynamics, should exhibit some characteristics behavior such as acceleration, stagnation and flow deflection, whose features are seem to be well captured by the numerical solutions depicted in Fig. 8. As mentioned previously, the velocity distribution at the free surface has been computed with the hydrostatic and non-hydrostatic 3D models, in conjunction with the zero-equation and two-equations standard k–ε models. Further insight into the

complex flow pattern can be observed in Fig. 9, where the formation of a separation zone deviates the flow towards the left bank at the inlet of the navigation channel.

Computed secondary flow patterns in XS-2, a bit downstream of the difluence (see Fig. 5 for surveyed cross-sections) are showed in Fig. 10. The results obtained with the hydrostatic and non-hydrostatic 3D models, in conjunction with the zero-equation and two-equations standard k–ε models show some variations along the vertical distribution of the streamwise velocity. Nevertheless, besides an optical effect due to the 3D projection algorithm used to plot the solution, the numerical results along XS-2 show a significant net unidirectional flow component in transverse direction from outer to inner regions [10]. This is induced by mass conservation to compensate the flow acceleration in the inner regions of the bend, clearly shown in the contour values of the flow module (see Fig. 10).

IV. CLOSURE

Since no unbiased algorithm is yet available to project the 3D computed velocity field onto the selected cross-sections [31], no judgment on the capability of the different mathematical models to fit observed data can be made at this point. Despite the increasing popularity of aDcp to study 3D flows, several issues must be overcome when matching observed cross-flow along bends with numerical results. One of this issues is related to the way the field data is captured and later treated, and the other is related with the use of different forms of the conservation laws and the effect the eddy viscosity model may have onto the solution. An unified algorithm to isolate cross-flow from a skewed discharge, either from field or numerical data, somehow is still lacking. Captured field data at some verticals (Fig. 6) resembles the cross-flow of Fig. 2. The figure of merit to judge the performance of different formulations of the governing equations of curved open-channel flows shouldn't be far from the simple model (1)–(3) solution.

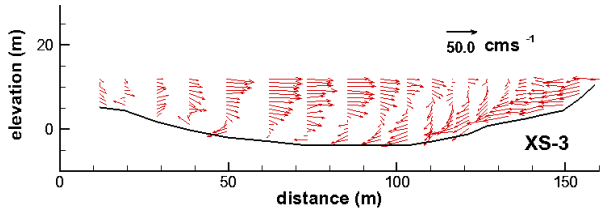

Figure 6. Transverse velocities along XS-3 captured with the Sontek aDcp, and processed with an in-house software.

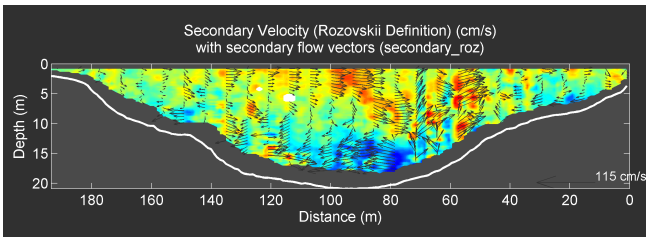

Figure 7. Transverse velocities along XS-3 captured with the TRDI aDcp, and processed with the VMT [26].

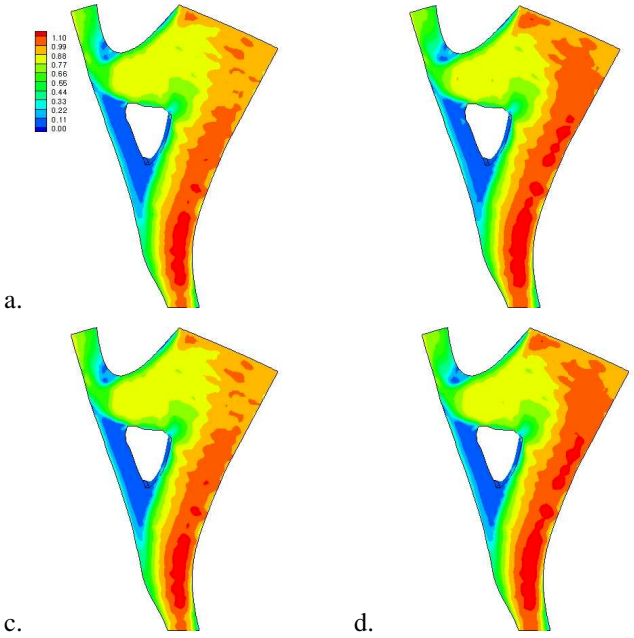

Figure 8. Velocity at the water surface (in ms^{-1}). Snapshots (a) and (b): 3D hydrostatic + zero and 2 k-e turbulence models resp. Snapshots (c) and (d): 3D non-hydrostatic + zero and k-e turbulence models, respectively.

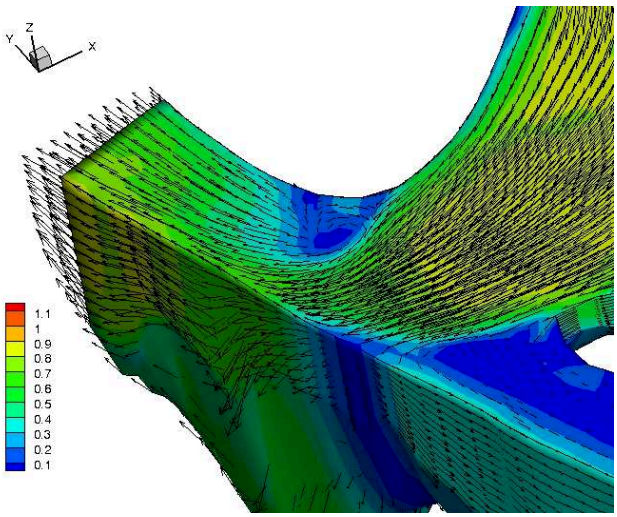

Figure 9. Velocity field and module (in ms^{-1}) at the separation zone.

ACKNOWLEDGEMENT

Support from CONICET and UNL, and EDF R&D as well, is gratefully acknowledged.

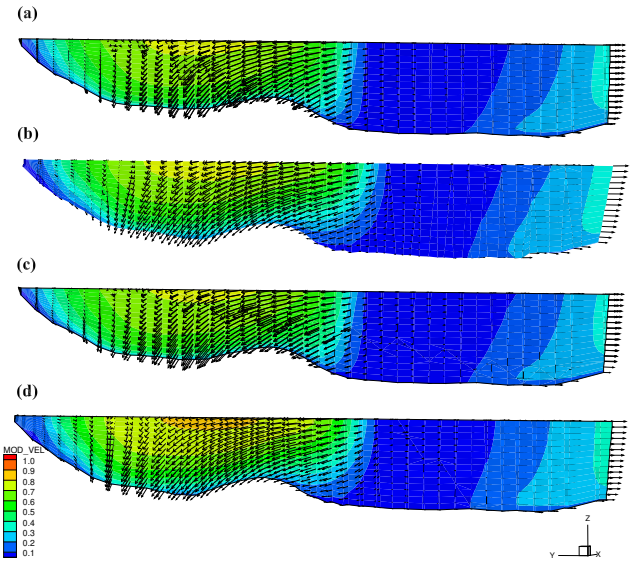

Figure 10. Secondary flow patterns in cross-section XS-2 upstream the difluence; (a) and (b): 3D hydrostatic model + zero and two equations *k*–ε turbulence models resp.; (c) and (d): 3D non-hydrostatic model + zero and two equations *k*–ε turbulence models resp.

REFERENCES

[1] Engelund F., "Flow and bed topography in channel bends", J. Hydrau. Div. ASCE, 1974, 100(11), pp. 1631-1648.

[2] Dietrich W.E., and Smith J. D., "Influence of the point bar on flow through curved channels", Water Resour. Res., 1983, 19(5), pp. 1173-1192.

[3] Blanckaert K., Schnauder I., Sukhodolov A., van Balen W., and Uijttewaal W.S.J., "Meandering: Field experiments, laboratory experiments and numerical modeling", In: RCEM 2009, pp. 863-875, Vionnet et al. (eds), Taylor & Francis Group, London.

[4] Stronach J.A, Backhaus J.O, and Murty T.S., "An update on the numerical simulation of oceanographic processes in the waters between vancouver island and the mainland: the GF8 model", Oceanogr. Mar. Biol. Annu. Rev., 1993, 31, pp. 1-86.

[5] Rodi W., "Turbulence Models and their Application in Hydraulics, A state-of-the-art review", IAHR Monograph, 3rd Edition, A.A. Balkema, Rotterdam, 1993, pp. 104.

[6] Seminara G., Zolezzi G., Tubino M., and Zardi D., "Downstream and upstream influence in river meandering. Part 2: Planimetric development", J. Fluid Mech, 2001, 438, pp. 213-230.

[7] Johannesson H., and G. Parker, "Secondary flow in mildly sinuous channels", J. Hydraulic Eng., 1989, 115(3), pp. 289-308.

[8] Duan J.G., and P.Y. Julien, "Numerical simulation of inception of channel meandering", Earth Surf. Process. Landforms, 2005, 30, pp. 1093–1110.

[9] Yalin M.S., "River mechanics", Pergamon Press Ltd, Oxford, UK, 1992.

[10] Tarrab L., M.G. Gallego, M.I. Morell, C.J. Ocampo, and C.A. Vionnet, "Measuring the super-elevation phenomena in coincidence with secondary currents induce by centrifugal effects", In: RCEM 2009, pp. 1023-1030, Vionnet et al. (eds), Taylor & Francis Group, London.

[11] Vionnet C.A., and J.C. Heinrich, "Penalty modeling of flows influenced by body forces", Proc. VIII Int. Conf. Finite Element in Fluids: New trends and applications, K. Morgan, E. Onate, J. Periaux, J. Peraire, O.C. Zienkiewics (eds.), Pineridge Press, 1, pp. 174-183, CIMNE, Barcelona, Spain, Aug 23-27, 1993

[12] Rozovskii I.L., "Flow of Water in Bends of Open Channels". Academy of Sciences of the Ukrainian SSR: Kiev, 1957 (translated from Russian by the Israel Program for Scientific Translations, Jerusalem, 1961).

[13] Parker G., E.C. Eke, and Y. Shimizu, "Steady, uniform bend flow over an erodible bed with transverse bedload flux: a window to the process of meander migration", In: RCEM 2009, pp. 111-117, Vionnet et al. (eds), Taylor & Francis Group, London

[14] Dinehart R.L., and J.R. Burau, "Repeated surveys by acoustic Doppler current profiler for flow and sediment dynamics in a tidal river", J. Hydrol., 2005, pp. 314, 1-21.

[15] Hickin, E.J., "Mean flow structure in meanders of the Squamish River, British Columbia", Can. J. Earth Sci., 1978, 15, pp. 1833-1849.

[16] Muste M., K. Yu, and M. Spasojevic, "Practical aspects of ADCP data use for quantification of mean river flow characteristics; Part I: moving-vessel measurements", Flow Measurement and Instrumentation, 2004, 15(1), pp. 1-16.

[17] Szupiany, R. N., M. L. Amsler, J. L. Best, and D. R. Parsons, "Comparison of fixed- and moving vessel measurements with an aDp in a large river", J. Hydraul. Eng., 2007, 133(12), pp. 1299–1310.

[18] Hervouet, J-.M., "Hydrodynamics of Free Surface Flows. Modelling with the finite element method", John Wiley & Sons, Ltd, 2007.

[19] Quarteroni, A., "Numerical models for differential problems", Modeling, Simulation & Applications series, vol. 2. Springer-Verlag Italia, Milan, 2009.

[20] www.opentelemac.org

[21] Decoene, Astrid, "Modèle hydrostatique pour les écoulements à surface libre tridimensionnels et schémas numériques", Ph.D. Thesis, Université Paris VI, 2006.

[22] Burchard, H., "Applied turbulence modelling in marine waters", Lecture Notes in Earth Sciences, Springer-Verlag, 2002.

[23] Wu, W., "Computational river dynamics", Taylor & Francis, Inc., 2007.

[24] SMS, Surface Modeling System – User's Manual, EMRL, Brigham Young University, Utah, U.S.A, 2000.

[25] Tecplot, User's Manual for Tecplot 360TM Version 2011, Tecplot, Inc., Bellevue, WA, U.S.A, 2011.

[26] Parsons, D. R., P. R. Jackson, J. A. Czuba, K. Oberg, J. L. Best, B. L. Rhoads, F. Engel, and J. D. Riley, "Velocity mapping toolbox (VMT): a new post-processing suite for acoustic doppler current profiler data", Earth Surf. Processes Landforms, submitted, 2011.

[27] Vionnet, C.A., "River bed topography; interpolation of scatter data", Internal Report CENEHA 01-2010, FICH, UNL, Santa Fe, Argentina, 2010.

[28] Sontek/YSI, RiverSurveyor System Manual, Software v.4.10, San Diego, CA, U.S.A, 2004.

[29] Snyder, J.P., Map projections – a working manual. Profess. Paper 1395, U.S.G.S., Washington DC 20402, U.S.A, 1929.

[30] Teledyne RD Instruments, WinRiver II, User's Guide, Poway, CA, U.S.A, 2007.

[31] Morell, M.I., and Vionnet, C.A., "On the Rozovskii method to isolate secondary circulation from skewed flow", to be submitted, 2011.

[32] Mourad F., personal communication.